IEEE Access
Multidisciplinary ⋮ Rapid Review ⋮ Open Access Journal

Received 25 April 2024, accepted 19 May 2024, date of publication 23 May 2024, date of current version 3 June 2024.

Digital Object Identifier 10.1109/ACCESS.2024.3404498

RESEARCH ARTICLE

Experiments and Study of a Low-Frequency, High-Speed Bi-Directional Piezoelectric Stick-Slip Actuator

XIAOCHAO TIAN, JIE YANG, HOUJUN GAI, JUNJIE LI, ZHENMING WANG, YINGYU DAI, AND DEFENG NIU

School of Vehicle and Mechanical Engineering, Changchun University, Changchun 130022, China

Corresponding author: Xiaochao Tian (txczb@163.com)

This work was supported by the Natural Science Foundation Program of Jilin Provincial Science and Technology Department under Grant 20240101096JC.

ABSTRACT In order to solve the problem of limited driving speed of piezoelectric actuators when the piezoelectric components are small and the driving frequency is low. This paper proposes a bi-directional piezoelectric stick-slip actuator, which mainly utilizes the combination of flexible drive foot and lever amplification mechanism to realize the displacement amplification function, thus improving the driving performance. Firstly describe the structure and working principle of the proposed actuator, and carries out theoretical analysis and mathematical modeling of the flexible stator. Then the driving process of the proposed actuator is simulated and analyzed with COMSOL Multiphysics simulation software, and the feasibility of the driver structure is preliminarily verified. Finally, establish an experimental system to test the basic characteristics of the prototype. The experimental results confirm that under the piezoelectric stacks elongation of 5μm, the driving frequency of 610Hz, the maximum drive speed of the actuator is 11.21mm/s. The maximum load capacity is 0.78N and the forward and backward displacement deviation within 10 cycles is 0.99μm under the locking displacement of 10μm. The proposed stick-slip actuator is capable of realizing a large driving speed when the elongations of the piezoelectric stacks are small and the driving frequency is low.

INDEX TERMS Stick-slip actuators, high speed, piezoelectric stack, bi-directional drive.

I. INTRODUCTION

With the rapid development of precision and ultra-precision machining, precision optical instruments, biomedical equipment, aerospace engineering and other fields [1], [2], [3], [4], [5], piezoelectric actuators have received the attention of scholars around the world because of their fast response speed, high accuracy, and no electromagnetic interference [6], [7], [8], [9], [10], and are widely used in various fields [11], [12], [13]. When a piezoelectric stick-slip actuator is in operation, a drive signal is applied to the piezoelectric stacks to make them periodically expand and contract, which in turn creates static friction between the actuator and the slider to move the slider forward (the ''stick'' stage) and kinetic friction to move it backward (the ''slip'' stage). Through the accumulation of microscopic displacements within each signal cycle, a macroscopic driving effect is eventually achieved [14], [15], [16].

In order to make the piezoelectric actuators have better driving performance, many scholars have made various improvements to the piezoelectric actuators. Wang et al. Proposed a bi-directional piezoelectric actuator [17] with a maximum speed of 0.742 mm/s under the excitation signal of 100 V, 1000 Hz. Peng et al. proposed a piezoelectric stick-slip linear actuator with dual-target localization accuracy [18], which energizes the solenoid periodically to achieve the backward motion suppression, and achieves a maximum speed of 4.8 mm/s, under the excitation signal of 64V, 40KHz. Lu et al. proposed a piezoelectric actuator with a triangular displacement amplification mechanism [19], and

The associate editor coordinating the review of this manuscript and approving it for publication was Jingang Jiang.

the maximum output speed of the actuator was 20.17 mm/s under the excitation signal of 100 V, 610 Hz. Li et al. proposed a new piezoelectric actuator using a two-stage flexible hinge [20] with a maximum driving speed of 354.55 mm/s at a driving voltage of 150 V, 4.7 kHz. Li et al. proposed a piezoelectric actuator with two umbrella bending mechanisms [21], by which the two driving feet cooperate with each other in order to increase the driving speed, and the maximum speed of the actuator is 1.132 mm/s under the excitation signal of 120 V, 400 Hz. Li et al. proposed a piezoelectric actuator with an equilateral triangular mechanism [16] that utilizes parasitic motion for actuation, with a maximum actuation speed of 0.18 mm/s under the excitation signal of 100 V, 225 Hz. Li et al. proposed a bi-directional piezoelectric stick-slip actuator [22] with a drive speed of 7.69 mm/s under the excitation signal of 100 V, 480 Hz. Gu et al. designed a separated stick-slip actuator [23] with a maximum drive speed of 3.467 mm/s under the excitation signal of 150 V, 1 kHz. Cheng et al. proposed a signal optimization method [24] for piezoelectric actuators, using the mixture of resonant and non-resonant drive signals, which resulted in a 147.23% increase in the actuator output speed with respect to the conventional sawtooth excitation. Yan et al. proposed a new structure piezoelectric actuator [25] modeled on the forefoot of a bionic praying mantis, and established a theoretical model of the complex hinge structure so that the error between the experimental results and the simulation results is not more than 4%, and the maximal speed of this actuator is 4491.38 mrad/s. Zhang et al. proposed a piezoelectric actuator with various anisotropic friction surfaces [26] so that the coefficient of friction of the working surface in the backward direction is smaller than that in the driving direction, which in turn reduces the backwardness and improves the driving speed. Sun et al. proposed a lever amplified piezoelectric actuator [27], which is unidirectionally driven by a piezoelectric stack providing locking force first and then driven by another piezoelectric stack. The maximum speed can reach 4.099mm/s.

Xinqi Tian et al. proposed a novel U-shaped stepping linear piezoelectric actuator with two driving feet and low motion coupling [28], which achieves a maximum thrust force of 189.7 N and a maximum speed of 273.4 μm/s.

The current piezoelectric actuators are mainly designed to increase the drive speed by increasing the drive frequency, using larger piezoelectric stack elongation, optimizing the excitation signal, optimizing the materials used or proposing new structures. but a higher drive frequency will lead to an increase in the piezoelectric stacks heat, and the large elongation of piezoelectric stacks will also affect the life of the actuators, optimizing the excitation signal will make the actuators control more complicated, optimizing the materials used will increase the processing difficulty of the actuator, and some of the new structures may increase the difficulty of the theoretical analysis and calculations of the actuator.

In summary, this paper proposes a piezoelectric stick-slip actuator that can realize bi-directional drive, made of 7075 aluminum alloy, using a structure that combines a flexible drive foot and a lever amplification mechanism, which is convenient for theoretical calculations and analysis. When the actuator is unidirectionally driving, it is driven using two smaller piezoelectric stacks that coupled with excitation signals of different waveforms, enable to actuate the actuator while providing locking force. The actuator has high drive speeds even at lower drive frequencies and with smaller piezoelectric stack elongations, and could be applied in the fields of machining and precision manufacturing.

II. ACTUATOR STRUCTURE AND DRIVING PRINCIPLE

A. ACTUATOR STRUCTURE

The overall structure of the actuator is shown in Figure 1, which mainly consists of a guide rail, a slider, a base, an adjustment platform, a preloading device and a stator, which consists of a flexible amplification mechanism and piezoelectric stacks (3mm × 3mm × 6mm) are embedded in the flexure amplification mechanism by means of spacers. The stator is mounted by means of screws on an adjustment platform that can slide along the y-axis, the adjustment platform consists of two parts, the lower part is connected to the base by screws and has a guiding function, and the upper part can be adjusted by the micrometer in the preloading device to maintain a certain locking displacement between the flexible stator and the slider. After the preloading device has corrected the position of the adjustment platform, the positioning screw on the side of the platform can be tightened to complete the positioning of the actuator.

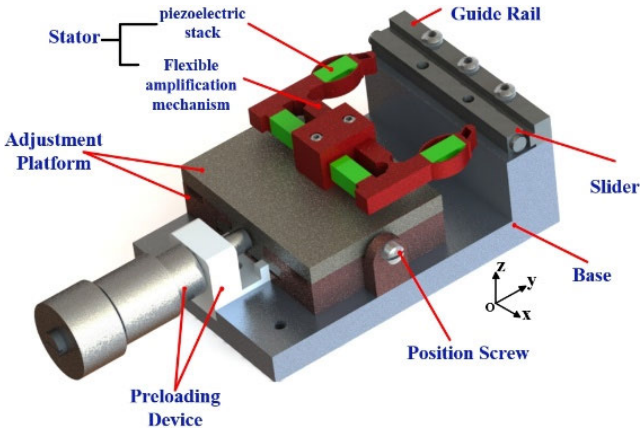

FIGURE 1. Schematic diagram of actuator structure.

B. DRIVING PRINCIPLE

According to the structure of the actuator, it can be seen that two piezoelectric stacks are required as the power source for unidirectional driving, and since the two piezoelectric stacks do not elongate at the same time, it is necessary to couple their

excitation signals. Figure 2 shows the driving principle of the actuator, taking the x-axis forward drive as an example, the driving process in one signal cycle can be divided into three stages.

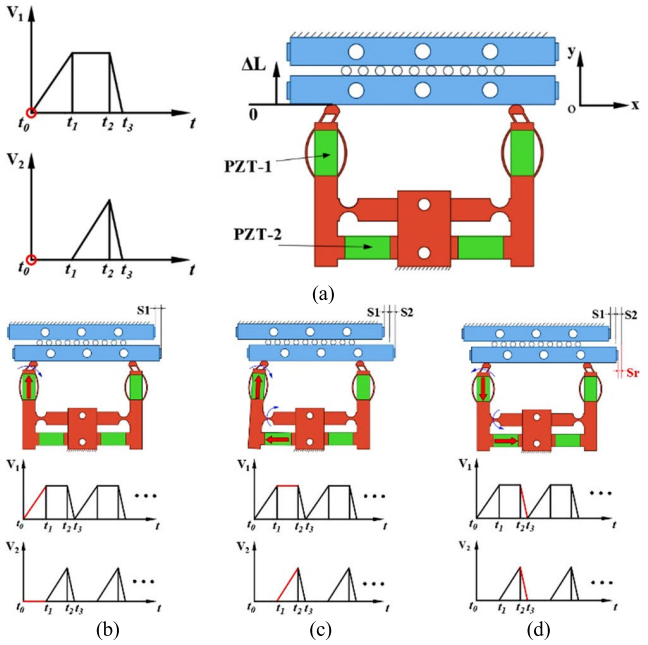

FIGURE 2. The driving process of the actuator. (a) Initial stage. (b) Drive foot deformation phase. (c) Lever amplification phase. (d) Voltage drop stage.

Initial stage: At t_0 time, no excitation signals are input to the piezoelectric stacks (PZT-1, PZT-2), and the locking displacement between the stator's flexible drive foot and the slider can be adjusted (remembering that the surface of the slider is a zero scale, and that the direction of the flexible stator away from the slider is in the negative direction).

Driving stage (b), (c): the driving stage is divided into two phases, t_0-t_1 moment is the drive foot deformation phase, PZT-1 elongates with the input of the excitation signal V_1, and due to the squeezing of the PZT-1 and the slider, the asymmetric flexible drive foot undergoes deformation as shown in Figure 2(b) and generates friction of positive x-axis direction with the slider, causing the slider to produce a displacement of S1. During this time period, the PZT-2 is not input an excitation signal. The t_1-t_2 moment is the lever amplification phase (c): the PZT-1 maintains the voltage of the t_1 moment, the PZT-2 gradually elongates with the input of the excitation signal V_2, and the lever amplification structure rotates clockwise around the flexible hinge, causing the slider to produce the displacement of S2.

Voltage drop stage (d): at the moment of t_2-t_3, the voltages of PZT-1 and PZT-2 drop rapidly at the same time, and the stator generates a sliding friction force on the slider in the opposite direction to the driving direction in a very short period of time, so that the slider generates a period of backward displacement Sr in the negative direction of the x-axis. At the moment t_3 the drive reverts to the state of the initial stage (a), and the effective displacement of the drive in one excitation signal cycle is

$$(S1 + S2) - Sr \tag{1}$$

By repeating the above three driving stages, the proposed piezoelectric stick-slip actuator can realize linear driving.

III. THEORETICAL CALCULATION

The main parameters of the stator are schematically shown in Figure 3. Since the elongation of the piezoelectric stacks are small, the deformation of the stator in the non-driven direction is also extremely small, so the theoretical displacement of the stator can be calculated using the pseudo-rigid body method. From the driving principle, it can be seen that the stator can be divided into two parts: the flexible drive foot and the lever amplification mechanism, so the superposition method can be used to calculate the displacement generated by these two parts respectively. The values of the main parameters of the stator are shown in Table 1.

The equivalent geometric model of the flexible drive foot is shown in Figure 3. Due to the elongation L_1 of the PZT-1 and the locking displacement ΔL, point C which is the midpoint of the bottom edge of the drive foot, will move to point C_1, and at the same time, point Q will move to point Q_1. Since the contact point $P_0$of the stator and the slider and the semicircular center Q of the flexible drive foot have the same trajectory, the displacement of point Q can be used to replace the displacement of the contact point P_0, if point C_1 is coincided with point C, the motion of the flexible drive foot can be regarded as a rotation of the rod CQ around point C.

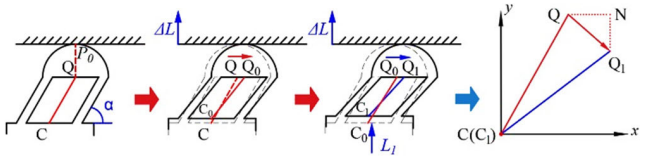

FIGURE 3. Equivalent geometric model of the flexible drive foot.

With point C as the origin to establish the right-angled coordinate system shown in Figure 4, the circle with C as the center of the radius of the circle expression is:

$$x^2 + y^2 = CQ^2 \tag{2}$$

Since there is a locking displacement ΔL between the drive foot and the slider, the Q drop height NQ_1 is $(L_1 + \Delta L)$. From the geometric relationship, the coordinates of Q are $(CQ \times \cos\alpha, CQ \times \sin\alpha)$, then the vertical coordinate of Q_1 are:

$$l_0 = CQ \times \sin\alpha - (L_1 + \Delta L) \tag{3}$$

Bringing (3) into (2) yields the horizontal coordinate of Q_1 as:

$$l_1 = \sqrt{CQ^2 - [CQ \times \sin\alpha - (L_1 + \Delta L)]^2} \tag{4}$$

Then QN is:

$$QN = l_1 - CQ \times \cos\alpha \tag{5}$$

Similarly, the horizontal deformation QQ_0 of the flexible drive foot caused by the locking displacement ΔL is:

$$QQ_0 = \sqrt{CQ^2 - [CQ \times \sin\alpha - \Delta L]^2} - CQ \times \cos\alpha \quad (6)$$

Therefore, the output displacement Q_0Q_1 of the actuator caused by the elongation of the PZT-1 is:

$$Q_0Q_1 = l_1 - QQ_0 \quad (7)$$

The lever amplification mechanism mainly amplifies the elongation L_2 of the PZT-2, and its equivalent geometric model is shown in Figure 4:

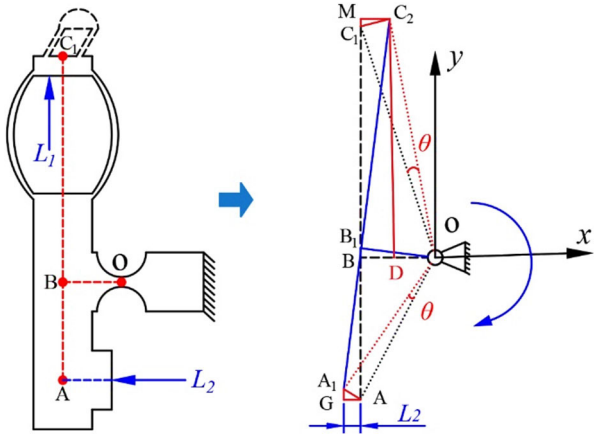

FIGURE 4. Equivalent geometric model of lever amplification mechanism.

Point O is the center of rotation of the flexible hinge, and point A rotates clockwise around point O by an angle θ under the push of PZT-2 and moves to point A_1. A right-angle coordinate system is established with point O as the origin, then the circle with radius OA can be defined as:

$$x^2 + y^2 = OA^2 \quad (8)$$

The horizontal coordinate of point A is -OB, then the horizontal coordinate of A_1 is -(OB + L_2) Bringing this into (8) gives the vertical coordinate of A_1:

$$l_2 = -\sqrt{OA^2 - (OB + L_2)^2} \quad (9)$$

(9) The length of A_1G can be obtained as (AB-l_2), then the length of A_1A is:

$$A_1A = l_3 = \sqrt{(AB - l_2)^2 + L_2^2} \quad (10)$$

The tiny angle θ of rotation of OA can be expressed as:

$$\theta = \arcsin\left(l_3 / OA\right) \quad (11)$$

From the geometric relationship, we know that OC_1 is also rotated clockwise by an angle θ around the point O, then can get:

$$C_2D = OC_2 \times \sin(\theta + \angle BOC) \quad (12)$$

$$OD = OC_2 \times \cos(\theta + \angle BOC_1) \quad (13)$$

$$MC_2 = OB - OD \quad (14)$$

$$MC_1 = C_2D - C_1B \quad (15)$$

At the same time, as the point C_1 produces a displacement MC_1 in the positive direction of the y-axis, which will cause further deformation of the flexible drive foot, the horizontal coordinate of Q_1 becomes:

$$l_1'' = \sqrt{CQ^2 - [CQ \times \sin 60° - (L_1 + \Delta L + MC_1)]^2} \quad (16)$$

Then the horizontal displacement Q_0Q_1 of the drive foot becomes:

$$Q_0Q_1' = l_1'' - CQ \times \cos 60° - QQ_0 \quad (17)$$

Therefore, the theoretical maximum step length L_M of the actuator in one signal cycle is:

$$L_M = MC_2 + Q_0Q_1' \quad (18)$$

The amplification ratios $\omega_{1,2}$ for the two driving phases are as follows:

Drive foot deformation phase:

$$\omega_1 = Q_0Q_1 / L_1 \quad (19)$$

Lever amplification phase:

$$\omega_2 = \left(MC_2 + Q_0Q_1' - Q_0Q_1\right) / L_2 \quad (20)$$

From the above calculation process, it can be seen that the locking displacement ΔL between the drive foot and the slider has a direct influence on the driving displacement of the flexible drive foot part: The larger ΔL is, the smaller is the displacement Q_0Q_1 produced by the drive foot deformation phase, at the same time, because the center of rotation of the lever amplification mechanism is outside the lever, the actuator in the lever amplification phase will certainly produce y-axis forward displacement MC_1, which can allow further. deformation of the drive foot to increase the step length of the actuator and the locking force in the driving process.

IV. DESIGN AND SIMULATION ANALYSIS

A. DIMENSIONAL DESIGN

To determine the dimensional parameters of the flexible drive foot, the characteristics of the actuator were analyzed using simulation software. Considering the size of the piezoelectric stacks as well as the structural strength and driving performance of the actuator, the thickness T of the flexible drive foot is designed to be 3 mm, the thickness t_1 of the connecting beam is designed to be 0.2 mm.

According to the THEORETICAL CALCULATION, the tilt angle α and the length l of the connecting beam have the greatest impact on the theoretical step length L_M, consider the driving performance and principle of the actuator as well as the structural strength, the tilt angle α of the connecting beam is in the range of [45°, 90°], and the length l of the connecting beam is in the range of [1.5 mm, 2.5 mm]. The material of the flexible amplification mechanism is 7075 aluminum alloy (Some of the properties are shown in Table 1), the material of the slider and guide rail is structural steel, the friction coefficient between the two

driving feet and the slider is 0.15, and the friction coefficient between the slider and the guide rail is 0.01. Setting the screw holes of the flexible amplification mechanism and the guide rails as fixed constraints, the locking displacement ΔL is 0 μm, and to better match the actual situation, the elongation of PZT-1 is set as 5μm. The rightward (x-axis positive direction) output displacements and stresses of the actuator of the drive foot deformation phase are simulated for different tilting angles and lengths of the connecting beams and the results of the computational analyses of the steady state are shown in Figure 5.

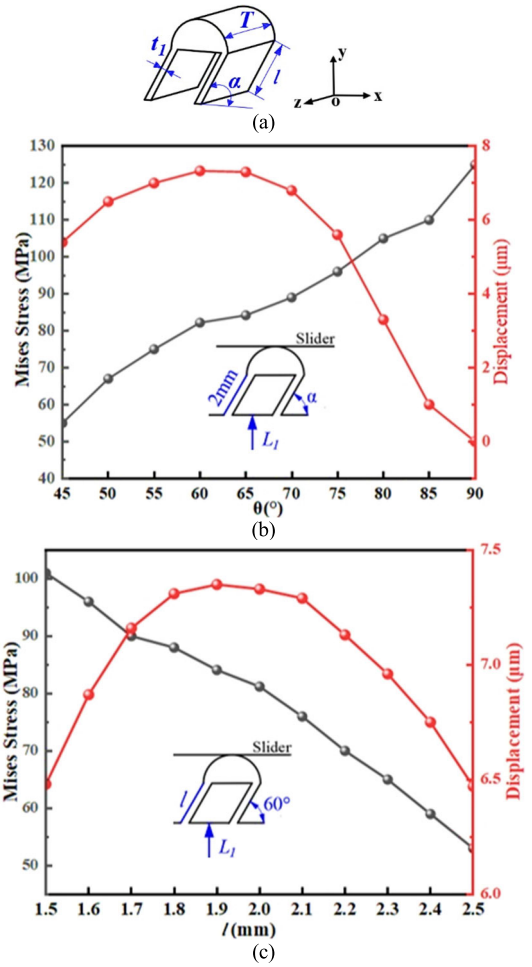

FIGURE 5. Dimension selection of the flexible drive feet. (a) Schematic diagram of drive foot dimensions. (b) Angle of inclination of connection beam α. (c) Length of connecting beam l.

Since both of these dimensions have an effect on the output performance of the actuator, the length of the connecting beam is first assumed to be 2 mm to determine the optimal tilt angle α. The determined α is then used to determine the optimal length l. From Figure 5, it can be seen that the stress in the flexible amplification mechanism increases with α. At this stage, the actuator relies on static friction to realize the drive, so when α is small, the stress generated by the drive foot is small, resulting in the friction between the slider and the drive foot is small and make them happen relative sliding, which reduces the output displacement of the actuator. When α is larger, due to the smaller inclination of the connecting beam, the stress is larger, and it is difficult for the drive foot to reach the theoretical deformation, so the output displacement of the actuator is also smaller at this time.In order to have a large output displacement and moderate stress, α is finally chosen to be 60°. The optimal connection beam length l when α is 60° is then selected, and similarly, the connection beam length is finally selected to be 1.9 mm. Considering the compactness of the driver and the dimensions of the piezoelectric stacks, the final dimensions of the lever amplification mechanism (Figure. 4) were chosen as AB=5mm, BC=11.5mm (before the extension of PZT-1), OB=3mm. The important dimensions of the stator are shown in Table 2.

TABLE 1. Properties of 7075 aluminum alloy.

Properties	Density	elastic modulus	Poisson's ratio
Value	2810kg/m^3	7.17×10^{4}MPa	0.33

TABLE 2. Stator dimensions.

Dimensions	BC	AB	OB	T	t_1	l	θ
Value(mm)	11.5	5	3	3	0.2	1.9	60°

B. STRESS AND STRAIN ANALYSIS

In order to verify the accuracy of the proposed calculation theory and the reliability of the actuator structure, the stress and strain of the stator in one excitation signal cycle are simulated and analyzed by driving the actuator to the right (x-axis positive direction) as an example. Keeping the constraints and actuator materials in the DIMENSIONAL DESIGN unchanged, the PZT-1 and 2 are set up in the solid mechanics physical field to elongate 5 μm successively in order to simulate the drive foot deformation phase and the lever amplification phase. In order to better fit the actual situation, the locking displacement between the stator and the slider is set to 10 μm, the coefficient of friction between the drive foot and the slider is set as 0.1 to make them maintain static friction during the driving stage and the coefficient of friction between the slider and the guide is set as 0.01 so that they could always maintain sliding friction. Finally, the steady state calculation and analysis is carried out, and the simulation results are shown in Figure 6.

From Figure 6, in the drive foot deformation phase, the contact point P_0 moves 8.29 μm in the positive direction of x-axis to P_1. In the lever amplification stage, P_1 moves to P_2, and finally the slider produces a horizontal displacement of 24.45 μm. The maximum stress generated by the deformation of the stator during the driving process is 99.1 MPa, which is much smaller than the permissible stress of 7075 aluminum alloy (505 MPa). From the simulation results, it can be seen that the proposed actuator has sufficient structural strength.

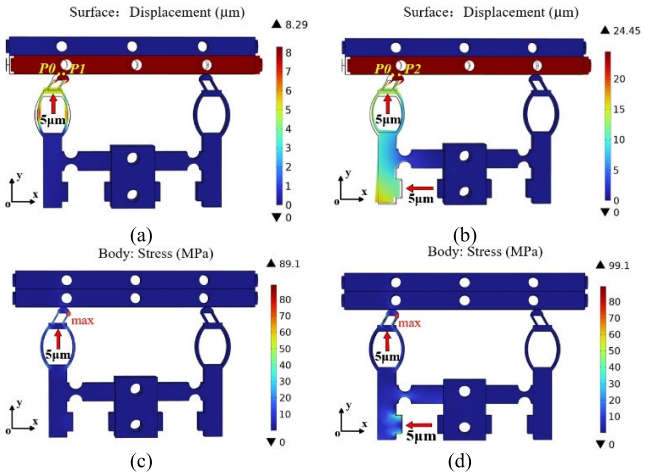

FIGURE 6. Stator stress-strain simulation (a) The stator strain of the drive foot deformation phase (b) The stator strain of the lever amplification stage (c) The stator stress of the drive foot deformation phase (d) The stator stress of the lever amplification phase.

Substituting the 5 μm elongation of PZT-1 and 2 into the theoretical equations and calculating the theoretical maximum output displacement of the stator in one signal cycle and comparing it with the simulation results, the results are shown in Table 3:

TABLE 3. Simulation and theoretical data.

Displacement (μm)	Simulation value	Theoretical value
P_0P_1	8.29	8.61
P_0P_2	24.45	24.9

According to Table 3, it can be seen that the error between the simulation value and the theoretical value is only 1.8%, which preliminarily verifies the accuracy of the theoretical calculation. From the structure of the actuator, it can be seen that the main cause of the error is the friction between the slider and the immobile drive foot.

In order to investigate the influence of the immobile drive foot on the output performance and further verify the accuracy of the theoretical calculations, the displacement excitation signals as the waveform shown in Figure 2 with a maximum value of 5 μm are inputted into the PZT-1 and PZT-2 positions respectively, and the dynamic simulation of the flexible stator is carried out. The maximum output displacement (MOD), theoretical output displacement (TOD), and effective displacement (EOD, the difference between MOD and backward displacement) of the flexible stator at different locking displacements ΔL are shown in Figure. 7.

From Figure 7, it can be seen that when ΔL is larger than 20 μm, the effective displacement of the flexible stator decreases rapidly, so the locking displacement of the actuator should not be larger than 20 μm. When ΔL is larger than 5 μm, the TOD is close to the MOD, and the maximum error is not more than 6%, and after ΔL is larger than 15 μm the error increases slowly, which is presumed to be the friction

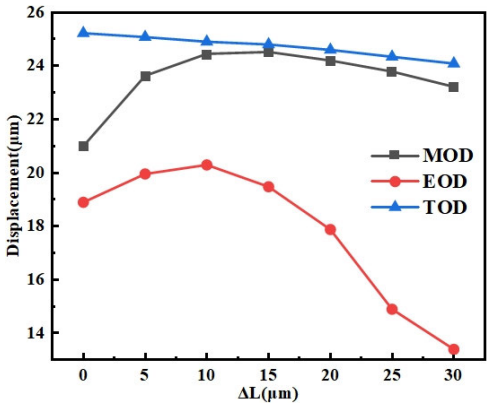

FIGURE 7. Output displacements at different ΔL.

of the immobile drive foot increases with the ΔL, and to a certain extent hinders the motion of the slider. When ΔL is 0, the friction between the stator and the slider is small resulting in more serious relative sliding. The simulation results verify the accuracy of the theoretical calculations and also show that the immobile drive foot has little effect on the output displacement of the actuator.

V. EXPERIMENTS AND ANALYSIS

A. EXPERIMENTAL SYSTEM

In order to further verify the driving performance of the proposed actuator, the actuator prototype was fabricated by using precision wire cutting machine, the materials of the actuator are 7075 aluminum alloy, and all the important dimensional parameters are the same as those in Table 1. And establish an experimental system as is shown in Figure 8.

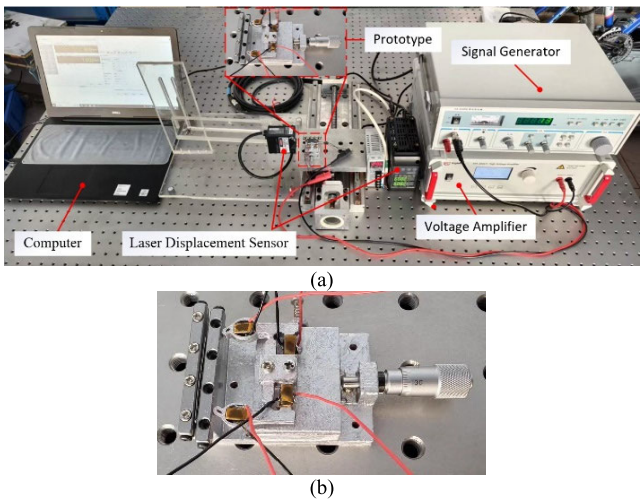

FIGURE 8. Experimental system (a)Experimental devices (b)the actuator prototype.

When the actuator realizes unidirectional driving, the excitation signals of different waveforms applied to the piezoelectric stacks (3mm × 3mm × 6mm, FTD150030306, Guangzhou Future Materials Technology Co., Ltd. The stroke

of the PZTs are approximately 5 μm with an applied voltage of 150 V.) are generated by a signal generator (SG030, Wuxi Shiao Technology Co., Ltd.) and applied to the piezoelectric stacks by a power amplifier (SA-PA010, Wuxi Shiao Technology Co., Ltd.).

The laser displacement sensor (LK-HD500-Keens) was fixed to a clamp made of an acrylic plate by means of fastening screws, and the drive step and output speed of the actuator were obtained by recording the position of a visor above the slider, and the data obtained from the experiment were processed by a computer. The actuator can be adjusted to align its position to the laser sensor by means of a small movable platform, and the distance between the stator and the slider can be adjusted by means of a preloading device. In the experiments, the piezoelectric stacks were driven with the excitation signals shown in Figure 2.

B. EXPERIMENTAL RESULT

Using the experimental system to test the performance of the actuator. The driving voltage U of PZT-1, PZT-2 is 150 V to ensure that the elongation is 5μm, and the output speed of the actuator is tested at different excitation frequencies and locking displacements ΔL. Taking drive to the right for example, the experimental results are shown in Figure 9:

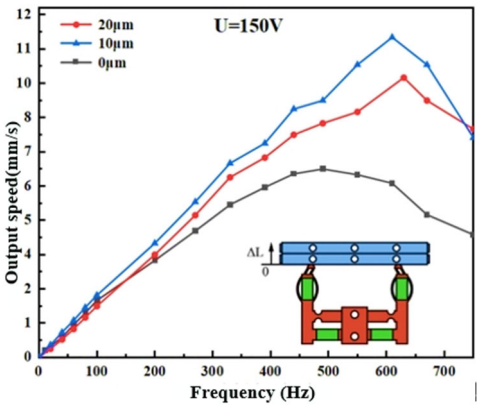

FIGURE 9. Relationship between drive frequency and output speed.

As can be seen from Figure 9, the output speed of the actuator under different locking displacements all show a trend of increasing and then decreasing. The peak velocity of the proposed actuator at the locking displacement of 0 is 6.2 mm/s, corresponds to a frequency of about 490 Hz, at the locking displacements of 10 μm and 20 μm, the peak velocities are 11.21 mm/s and 9.8 mm/s, correspond to a frequency of about 610 Hz and 630 Hz. The reason why the peak velocity frequency of the actuator is gradually increased is with the locking displacement increases, the overall stiffness of the actuator also gradually increases, that leads to an increase in the resonant frequency of the actuator, that's also means these peak velocity frequencies are very close to the resonant frequencies of the actuator, and as the drive frequencies move away from the resonant frequency and the hysteresis effect of piezoelectric stacks, the output speed of the actuator begins to decrease, so the drive frequency of the actuator should not be higher than these peak frequencies in practical application.

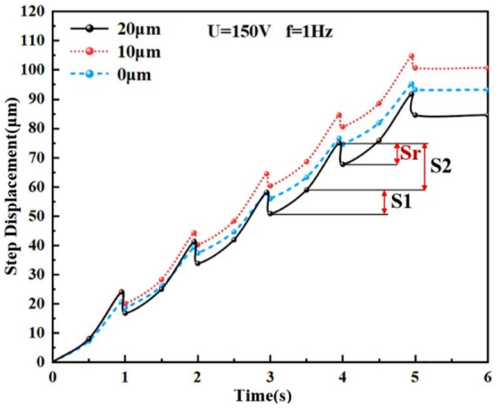

FIGURE 10. Step displacement of different locking displacements.

From the experimental results, with the increase of the locking displacement, the width of the stable operation frequency is also increasing, so in some cases we can increase the locking displacement to increase the load capacity and stability of the actuator.

Figure 10 shows the step displacement curves of the actuator at three different locking displacements under the low-frequency driving signal of 150 V and 1 Hz are all sawtooth-shaped. With the increase of the locking displacement, the average single maximum stepping displacements (S1+S2) of the actuator are about 20.63 μm, 24.38 μm, and 24.25 μm, and the average backward displacements Sr are about 2.04 μm, 4.02 μm, and 7.12 μm, during the test time of 5s. The sliding friction of the flexible stator during the backward movement is increased with the increase of the locking displacement, which resulting in an increase in the backward displacement Sr. Since the driving stage contains the drive foot deformation phase and the lever amplification phase, the displacement of the driving stage is divided into S1 and S2, from the driving process of the actuator and theoretical calculations and simulations, it is clear that S1 is always prior to and smaller than S2. From equation (1), the average effective step displacements of the actuator are 18.59 μm, 20.36 μm, and 17.13 μm of the three locking displacements, respectively. The experimental results also confirmed the accuracy of the theoretical calculations and simulation results.

TABLE 4. Comparison with previous actuators.

Source	Elongation(μm)	Frequency (Hz)	Load(N)	Speed(mm/s)
[17]	10	1000	36	0.742
[20]	20	4.7k	30	354.55
[22]	10	480	1.05	7.69
[23]	5	1000	20	3.467
[27]	10	110	10.01	4.099
[28]	32.6	6.25	189.7	0.2734
prototype	5	610	0.78	11.21

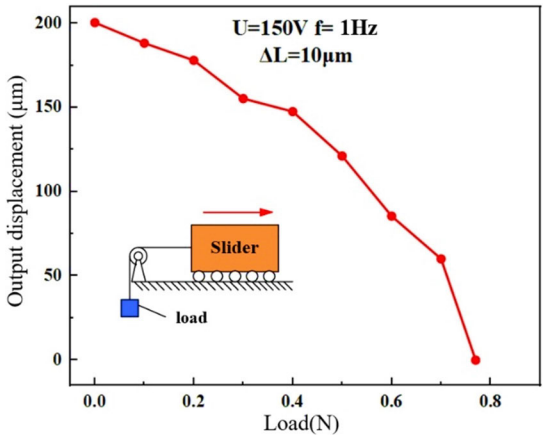

FIGURE 11. Relationship between load and displacement.

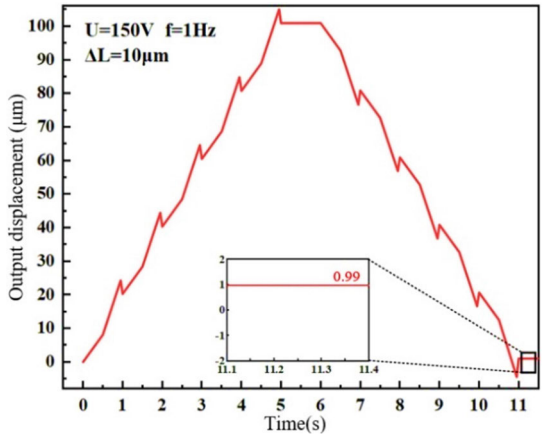

FIGURE 12. Reciprocating motion accuracy test.

From the two aforementioned experiments, it can be seen that the output performance of the actuator is better when the locking displacement is 10 μm, so the load performance of the actuator is tested by keeping the locking displacement of 10 μm. In 150V, 1Hz excitation signal, apply standard weights to the slider to test the total output displacement under different loads in 10s, the results are shown in Figure 11, with the increase of the load, the output displacement of the actuator is also gradually reduced, when the load is greater than 0.78N, the output displacement of the actuator is basically zero, so the maximum load of the actuator is 0.78N.

Reciprocating motion accuracy is one of the most important indicators of performance of actuators. During the test, the locking displacement ΔL of the actuator is kept at 10μm, and the laser sensor is used to measure and record the displacement difference of the final position of the slider compared to the starting position after 5 signal cycles of each for left and right motion of the actuator. The results are shown in Figure 12. During the test, after the original 5s test, wait for 1s and then start testing the reverse motion test. At the end of the 11s test, the displacement deviation of the slider relative to the starting point is 0.99μm.

Table 4 compares some of the output performances of the proposed piezoelectric actuator with the previous ones, and it can be seen that the proposed actuator is capable of realizing high-speed driving at low-frequency excitation signals.

VI. CONCLUSION

A bi-directional piezoelectric stick-slip actuator is proposed in the paper. After theoretical analysis and calculation, it can realize high-speed drive in the case of small piezoelectric stack elongation and low driving frequency. In order to verify the superiority of the performance of proposed actuator, the prototype of the actuator is fabricated, and an experimental platform is established to test the output performance, and the realization results show that, the maximum load of the proposed actuator is 0.78N, and the deviation of reciprocating displacement of 10 signal cycles is 0.99μm when the driving frequency is 610Hz, the piezoelectric stack elongation is 5 μm, and the locking displacement is 10 μm, the maximum output speed of the actuator is 11.21mm/s. Compared with the previous piezoelectric actuators, the proposed actuator can realize high output speed at low driving frequency.

REFERENCES

[1] J. Deng, Y. Liu, J. Liu, D. Xu, and Y. Wang, "Development of a planar piezoelectric actuator using bending–bending hybrid transducers," *IEEE Trans. Ind. Electron.*, vol. 66, no. 8, pp. 6141–6149, Aug. 2019.

[2] Q. Gao, M. He, X. Lu, C. Zhang, and T. Cheng, "Simple and high-performance stick-slip piezoelectric actuator based on an asymmetrical flexure Hinge driving mechanism," *J. Intell. Mater. Syst. Struct.*, vol. 30, no. 14, pp. 2125–2134, Aug. 2019.

[3] T. Cheng, M. He, H. Li, X. Lu, H. Zhao, and H. Gao, "A novel trapezoid-type stick–slip piezoelectric linear actuator using right circular flexure Hinge mechanism," *IEEE Trans. Ind. Electron.*, vol. 64, no. 7, pp. 5545–5552, Jul. 2017.

[4] Y. Wang, W. Chen, J. Deng, J. Li, and Y. Liu, "Toward compact motorized lens: Switch and focus a filter wheel with single piezoelectric tube," *Adv. Mater. Technol.*, vol. 9, no. 1, Jan. 2024, Art. no. 2301066.

[5] S. Izuhara and T. Mashimo, "Design and characterization of a thin linear ultrasonic motor for miniature focus systems," *Sens. Actuators A, Phys.*, vol. 329, Oct. 2021, Art. no. 112797.

[6] M. Hunstig, "Piezoelectric inertia motors—A critical review of history, concepts, design, applications, and perspectives," *Actuators*, vol. 6, no. 1, p. 7, Feb. 2017.

[7] C. Shi, D. K. Luu, and Q. Yang, "Recent advances in nanorobotic manipulation inside scanning electron microscopes," *Microsyst. Nanoeng.*, vol. 2, Jun. 2016, Art. no. 16024.

[8] Z. M. Zhang, Q. An, J. W. Li, and W. J. Zhang, "Piezoelectric friction–inertia actuator—A critical review and future perspective," *Int. J. Adv. Manuf. Technol.*, vol. 62, nos. 5–8, pp. 669–685, Sep. 2012.

[9] B. E. Kratochvil, L. Dong, and B. J. Nelson, "Real time rigid body visual tracking in a scanning electron microscope," *Int. J. Robot. Res.*, vol. 28, pp. 498–511, Apr. 2009.

[10] Y. Tian, D. Zhang, and B. Shirinzadeh, "Dynamic modelling of a flexure-based mechanism for ultra-precision grinding operation," *Precis. Eng.*, vol. 35, no. 4, pp. 554–565, Oct. 2011.

[11] Y. Liu, L. Wang, Z. Gu, Q. Quan, and J. Deng, "Development of a two-dimensional linear piezoelectric stepping platform using longitudinal-bending hybrid actuators," *IEEE Trans. Ind. Electron.*, vol. 66, no. 4, pp. 3030–3040, Apr. 2019.

[12] H. Li, J. Liu, K. Li, and Y. Liu, "Piezoelectric micro-jet devices: A review," *Sens. Actuators A, Phys.*, vol. 297, Oct. 2019, Art. no. 111552.

[13] M. Hunstig, "Piezoelectric inertia motors—A critical review of history, concepts," *Actuators*, vol. 6, no. 1, p. 7, 2017.

[14] F. Dubois, C. Belly, A. Saulot, and Y. Berthier, "Stick-slip in stepping piezoelectric inertia drive motors—Mechanism impact on a rubbing contact," *Tribol. Int.*, vol. 100, pp. 371–379, Aug. 2016.

[15] N. Wan, J. Wen, Y. Hu, J. Kan, and J. Li, "A parasitic type piezoelectric actuator with an asymmetrical flexure Hinge mechanism," *Microsyst. Technol.*, vol. 26, no. 3, pp. 917–924, Mar. 2020.
[16] J. Li, S. Chen, G. Zhao, J. Wen, and N. Wan, "A linear piezoelectric actuator with the parasitic motion of equilateral triangle flexure mechanism," *Smart Mater. Struct.*, vol. 29, no. 1, Jan. 2020, Art. no. 015015.
[17] J. Wang, J. Li, Z. Xu, S. Wang, Z. Wang, B. Xu, Y. Sun, S. Liu, and H. Zhao, "Design, analysis, experiments and kinetic model of a high step efficiency piezoelectric actuator," *Mechatronics*, vol. 59, pp. 61–68, May 2019.
[18] Y. Peng, J. Cao, Z. Guo, and H. Yu, "A linear actuator for precision positioning of dual objects," *Smart Mater. Struct.*, vol. 24, no. 12, Dec. 2015, Art. no. 125039.
[19] X. Lu, Q. Gao, Y. Li, Y. Yu, X. Zhang, G. Qiao, and T. Cheng, "A linear piezoelectric stick-slip actuator via triangular displacement amplification mechanism," *IEEE Access*, vol. 8, pp. 6515–6522, 2020.
[20] Z. Li, L. Zhao, and X. Yu, "A novel stick-slip piezoelectric actuator based on two-stage flexible Hinge structure," *Rev. Sci. Instrum.*, vol. 91, no. 5, p. 91, May 2020.
[21] J. Li, J. Cai, J. Wen, J. Yao, J. Huang, T. Zhao, and N. Wan, "A walking type piezoelectric actuator with two umbrella-shaped flexure mechanisms," *Smart Mater. Struct.*, vol. 29, no. 8, Aug. 2020, Art. no. 085014.
[22] Y. Li, H. Li, T. Cheng, X. Lu, H. Zhao, and P. Chen, "Note: Lever-type bidirectional stick-slip piezoelectric actuator with flexible Hinge," *Rev. Sci. Instrum.*, vol. 89, no. 8, Aug. 2018, Art. no. 086101.
[23] S. Gu, P. Pan, J. Zhu, Y. Wang, F. Yang, and C. Ru, "A piezoelectric stick–slip drive nanopositioner with large velocity under high load," *AIP Adv.*, vol. 10, no. 10, Oct. 2020, Art. no. 1105027.
[24] T. Cheng, H. Li, M. He, H. Zhao, X. Lu, and H. Gao, "Investigation on driving characteristics of a piezoelectric stick–slip actuator based on resonant/off-resonant hybrid excitation," *Smart Mater. Struct.*, vol. 26, no. 3, Mar. 2017, Art. no. 035042.
[25] L. Yan, J. Wang, T. Liang, D. Mao, B. Tong, C. Wang, H. Li, and H. Zhao, "A dual-mode stick-slip piezoelectric actuator imitating mantis forefoot," *Int. J. Mech. Sci.*, vol. 266, Mar. 2024, Art. no. 108985.
[26] Q. S. Zhang, X. B. Chen, Q. Yang, and W. J. Zhang, "Development and characterization of a novel piezoelectric-driven stick-slip actuator with anisotropic-friction surfaces," *Int. J. Adv. Manuf. Technol.*, vol. 61, nos. 9–12, pp. 1029–1034, Aug. 2012.
[27] M. Sun, W. Huang, Y. Wang, Q. Lu, and Z. Su, "Research on a novel non-resonant piezoelectric linear motor with lever amplification mechanism," *Sens. Actuators A, Phys.*, vol. 261, pp. 302–310, Jul. 2017.
[28] X. Tian, B. Zhang, Y. Liu, S. Chen, and H. Yu, "A novel U-shaped stepping linear piezoelectric actuator with two driving feet and low motion coupling: Design, modeling and experiments," *Mech. Syst. Signal Process.*, vol. 124, pp. 679–695, Jun. 2019.

XIAOCHAO TIAN was born in Heilongjiang, China, in 1986. He received the Ph.D. degree in mechanical engineering from Jilin University, Jilin, China, in 2016. Since 2015, he has been a Professor with Changchun University, Jilin. He has published more than 20 SCI articles. His research interests include piezoelectric precision drive and control technology, principles and applications of piezoelectric energy capture technology, and microfluidic technology research.

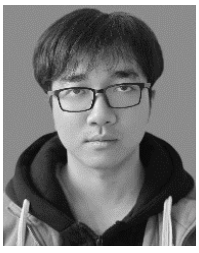

JIE YANG was born in Sichuan, China, in 1998. He received the B.S. degree from Qinghai University. He is currently pursuing the M.S. degree in mechanical engineering with Changchun University. His research interest includes piezoelectric actuators.

HOUJUN GAI was born in Shandong, China, in 1999. He received the B.S. degree in mechanical engineering from the College of Intelligent Equipment, Shandong University of Science and Technology, in 2021. He is currently pursuing the master's degree in mechanical engineering (with a focus on piezoelectric precision actuators) with the School of Mechanical and Vehicle Engineering, Changchun University.

JUNJIE LI was born in Shandong, China, in 1999. He received the B.S. degree in mechanical engineering from the School of Mechanical and Vehicle Engineering, Yantai Institute of Science and Technology, in 2022. He is currently pursuing the master's degree in mechanical engineering (with a focus on piezoelectric precision actuators) with the School of Mechanical and Vehicle Engineering, Changchun University.

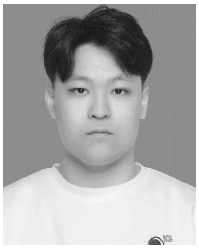

ZHENMING WANG was born in Liaoning, China, in 1999. He received the B.S. degree from Shenyang Jianzhu University. He is currently pursuing the M.S. degree in mechanical engineering with Changchun University. His research interest includes piezoelectric actuators.

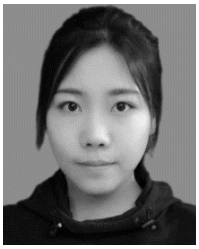

YINGYU DAI was born in Liaoning, China, in 2001. She received the B.S. degree from Shenyang Institute of Science and Technology. She is currently pursuing the M.S. degree in mechanical engineering with Changchun University. Her research interest includes piezoelectric sensors.

DEFENG NIU was born in Shandong, China, in 1998. He received the B.S. degree from Qingdao University of Science and Technology. He is currently pursuing the M.S. degree in mechanical engineering with Changchun University. His research interest includes piezoelectric sensors.